Total kinetic energy release in ^{239}Pu(n, f) post-neutron emission from 0.5 to 50 MeV incident neutron energy

K. Meierbachtol,[1,*] F. Tovesson,[1] D. L. Duke,[1] V. Geppert-Kleinrath,[1] B. Manning,[1] R. Meharchand,[2] S. Mosby,[1] and D. Shields[1]

[1]*Los Alamos National Laboratory, Los Alamos, New Mexico 87545, USA*

[2]*Institute for Defense Analyses, Alexandria, Virginia 22311-1882, USA*

(Received 21 April 2016; revised manuscript received 6 July 2016; published 14 September 2016)

The average total kinetic energy ($\overline{TKE}$) in ^{239}Pu(n, f) has been measured for incident neutron energies between 0.5 and 50 MeV. The experiment was performed at the Los Alamos Neutron Science Center (LANSCE) using the neutron time-of-flight technique, and the kinetic energy of fission fragments post-neutron emission was measured in a double Frisch-gridded ionization chamber. This represents the first experimental study of the energy dependence of $\overline{TKE}$ in ^{239}Pu above neutron energies of 6 MeV.

DOI: 10.1103/PhysRevC.94.034611

I. INTRODUCTION

As a nucleus undergoes fission, large amounts of energy are released, primarily in the form of kinetic energy shared between the two fragments that form after scission. This energy release drives fission-based technologies such as nuclear reactors, making the average total kinetic energy release ($\overline{TKE}$) in neutron-induced fission of the major actinides an essential physical quantity for modeling such systems. In this work we measure, for the first time, the evolution of $\overline{TKE}$ with incident neutron energy above 6 MeV in ^{239}Pu(n, f). This provides an accurate measure of the $\overline{TKE}$ for 14-MeV incident neutrons, which is the characteristic energy of neutrons produced in deuterium-tritium (D-T) fusion.

Previous studies of $\overline{TKE}$ in ^{235}U and ^{238}U have shown a general decrease in this quantity as the incident neutron energy is increased [1,2], at least up to incident neutron energy $E_n =$ 30 MeV. These data also exhibit sudden changes in the overall trend close to the threshold energies for multichance fission. Previous work on ^{239}Pu only extends up to $E_n = 5.5$ MeV of incident neutron energy [3], and therefore gives no clear indication of whether this isotope behaves in a manner similar to uranium.

Recent modeling of $\overline{TKE}$ as a function of incident neutron energy includes work by Madland [4] and Lestone [5]. Madland used existing data to parametrize the dependency of the ^{239}Pu(n, f) $\overline{TKE}$ with the following linear equations for pre- and post-neutron emission:

$$\left\langle T_f^{\text{tot}} \right\rangle = (177.80 \pm 0.03) - (0.3489 \pm 0.02) E_n \quad \text{(MeV)}, \quad (1)$$

$$\left\langle T_p^{\text{tot}} \right\rangle = (175.55 \pm 0.03) - (0.4566 \pm 0.02) E_n \quad \text{(MeV)}, \quad (2)$$

where E_n is the incident neutron energy and $\langle T_f^{\text{tot}} \rangle$ and $\langle T_p^{\text{tot}} \rangle$ are the average total fission fragment kinetic energy before neutron emission and after neutron emission, respectively. Madland includes the caveat that the equations should not to be used above an E_n value of 5.5 MeV. The lack of existing data severely limits predictive modeling and applications above this energy regime. Lestone's work focuses on new predictions that include the complexities of multichance fission channels by incorporating measured and predicted cross sections for first-, second-, third-, and fourth-chance fission. Figure 4 in Ref. [5] shows the resulting prediction for $\overline{TKE}$ for ^{239}Pu(n, f). It should be noted that the data available at the time do not extend to the region of Lestone's prediction for increases in $\overline{TKE}$ due to multichance fission.

This work reports the results of measurements of the post-neutron emission $\overline{TKE}$ in the neutron-induced fission of ^{239}Pu for neutron energies from 0.5 to 50 MeV. Details of the experiment are discussed and the experimental results are compared to predictive modeling efforts.

II. EXPERIMENTAL METHOD

A double Frisch-gridded ionization chamber was used to measure $\overline{TKE}$. The detector consisted of a chamber 12 cm in diameter and 13.5 cm in length filled with P10 gas (90% argon, 10% methane) to 95 kPa in pressure at a flow rate of $<$0.1 l/min. A central cathode 11 cm in diameter separated the volume into two halves. The cathode also held the ^{239}Pu sample in place. The target contained 363.4 μg of Pu deposited onto a 100-μg/cm^2 carbon foil. The sample diameter was $\sim$1 cm. Each half of the detector contained an anode, 12 cm in diameter, for signal collection. The anodes were separated from the common cathode by Frisch grids with an active radius of 4.5 cm. The active volume of the detector allowed for a maximum fission fragment track length of approximately 5.4 cm. The signals from the cathode, anodes, and grids were all read out.

The wide range of neutron energies available from the neutron spallation targets at the Los Alamos Neutron Science Center (LANSCE) enabled this measurement. The 90-deg flight path at the Weapons Neutron Research Facility (WNR) [6] was used for the measurement, accessing neutrons with an energy range of 100 keV to $>$100 MeV with the largest flux between approximately 0.2 and 300 MeV. This flux allowed for high statistics data collection with a relatively small amount of sample material. The neutrons, created by

*meierbachtol@lanl.gov

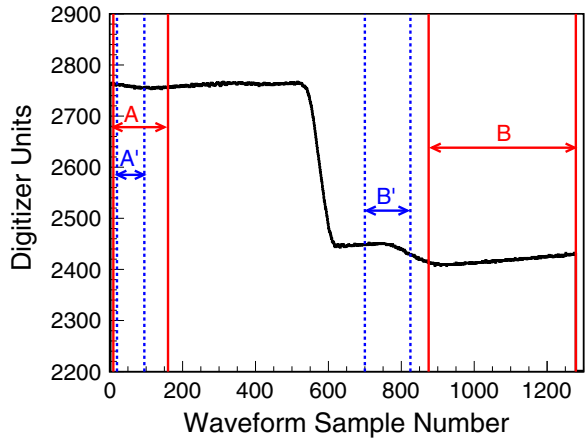

FIG. 1. Representative anode waveform signal. Baseline and decay regions for signal processing are indicated by arrows between two vertical lines. The original baseline and decay regions are label A and B while the modified regions are labeled A′ and B′, respectively.

spallation of 800-MeV protons from the LANSCE accelerator onto an unmoderated tungsten target, traveled 12.02 ± 0.01 m in air down the flight path collimation to the experimental setup. The timing structure of the neutron beam was a 40-pulses/s macropulse structure sampled from the 60-Hz accelerator frequency with 340 micropulses spaced 1.8 μs apart superimposed onto it. The time reference signal (T0) is taken from the proton beam pulse signal.

Data acquisition hardware for the experiment consisted of a CAEN VX1720 12-bit waveform digitizer with a sample rate of 250 MS/s [7]. The 5 signals from the detector (2 anode, 2 grid, and 1 cathode) were digitized as full waveforms along with the T0 signal. The anode and grid signals were processed by a charge-sensitive preamplifier prior to entering the digitizer. The cathode signal was processed with a fast amplifier. Details on operation of the digitizer and waveform collection can be found in Ref. [8].

The height of an anode signal is proportional to the fragment's kinetic energy. An exponential fit was applied to the waveform to determine the pulse height of the anode signal. To determine the limits of the fit, windows that set the flat baseline region prior to the signal and the decay region following the signal must first be identified. This is shown in Fig. 1 as regions A (baseline) and B (decay). However, this process was complicated by the presence of pileup due to α decays in the ^{239}Pu target, which cause additional structure in the waveforms. Figure 2 shows an example of a clean fission fragment anode signal in Fig. 2(a), and one contaminated by α decay in Fig. 2(b). Since α decay is a time-random process, fission fragment anode signals can be contaminated by a random number of α decay signals, making an accurate determination of the true pulse height challenging.

The windows around the baseline and decay regions that determine pulse height were modified to minimize the influence of α pileups that distort the fragment signal, shown in Fig. 1 as new regions A′ and B′. The baseline was sampled later in time for a shorter sampling period and the decay region was sampled earlier in time, also for a shorter

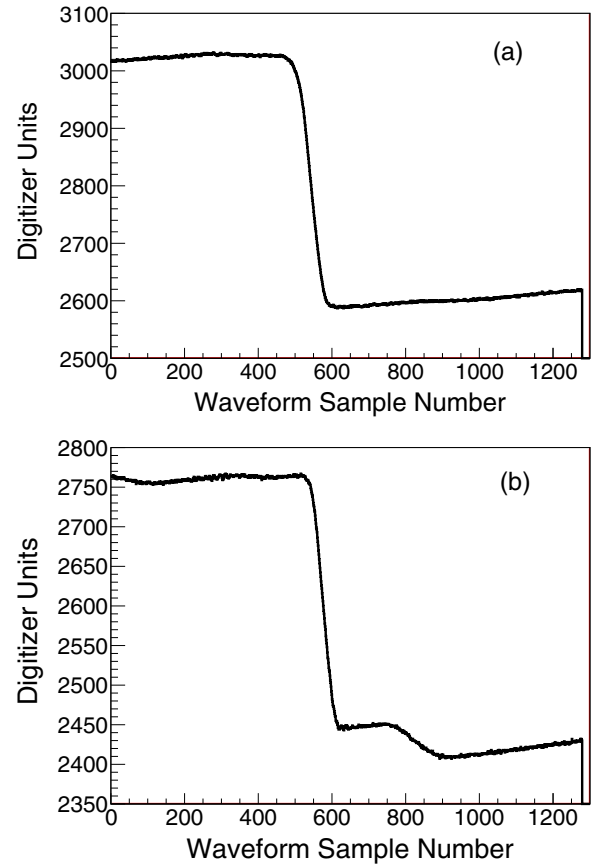

FIG. 2. Raw digitized waveforms from the anode plate signal for (a) a fission fragment without α particles and (b) a fission fragment and one α contamination in the signal decay.

sampling period. Approximately 60% of the anode signals had significant α pileup in the baseline and/or decay regions of the waveform. The window modifications significantly improved signal determination, resulting in 64% reduction in α contamination in the baseline sampling and a 63% reduction in the α contamination in the calculation of the pulse height, which is proportional to the fragment energy. Figure 3 illustrates the raw anode spectrum for one side of the detector before, Fig. 3(a), and after, Fig. 3(b), the corrections. Prior to correction of the regions used in waveform analysis, the anode spectrum was washed out and lacking the clear characteristic two peak structure of the light and heavy fission fragment energies. After adjustments, the two distinct peaks are restored with a valley in between.

Analysis of ^{239}Pu fission data are complicated by α pileup in the signals, which introduce uncertainty in fragment masses and pre-neutron energies in traditional 2E analyses (Refs. [8–10]). However, this work focuses on post-neutron emission $\overline{TKE}$ so many of the mass-dependent corrections required by 2E are unnecessary here. One such correction is the pulse height defect (PHD) in the gas. In this measurement, it is appropriate to choose a single PHD correction value and apply it for all fragment energies because the effect varies by less than 1% of the $\overline{TKE}$ over the range of fragment masses. Additionally, no correction is needed for the incident

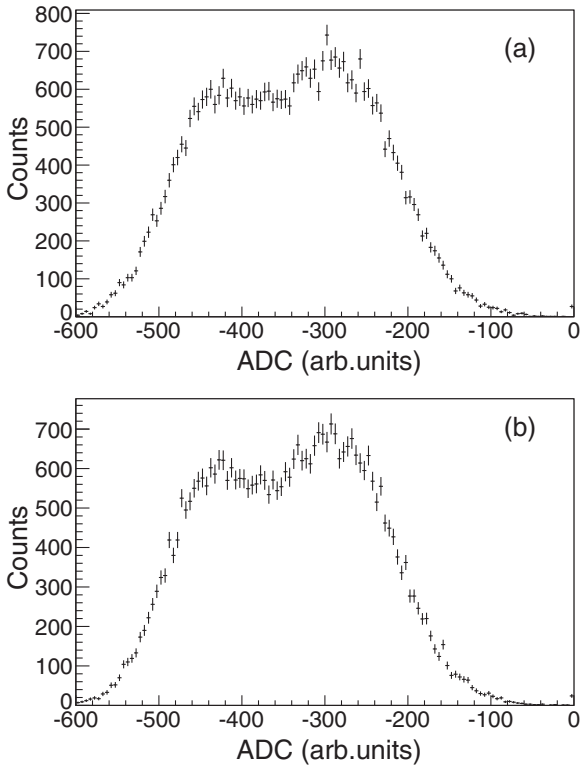

FIG. 3. Raw anode spectra for a subset of fission fragments (a) before and (b) after α contamination correction to raw waveforms.

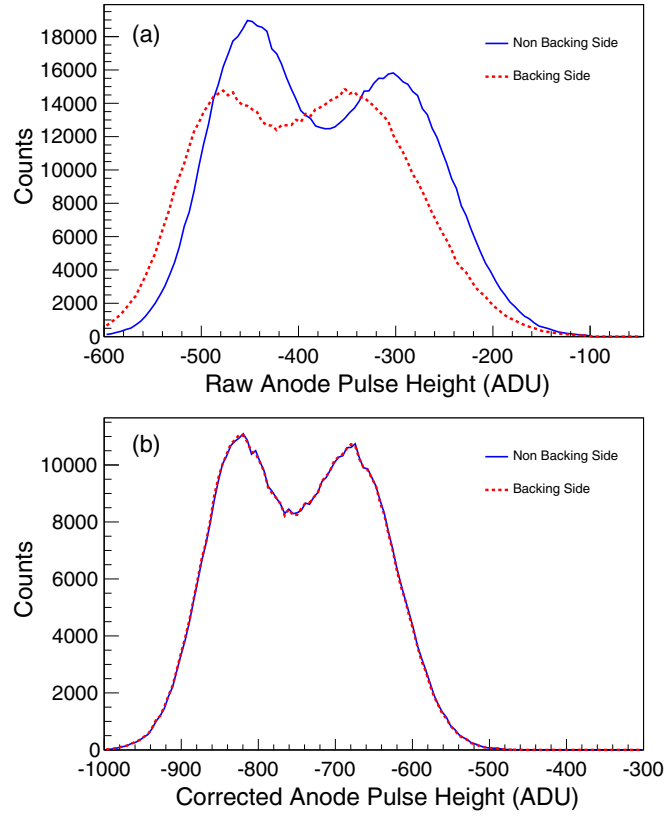

FIG. 4. Anode spectra for a subset of fission fragments (a) before and (b) after energy loss corrections in target backing material and gain matching of the backing side anode to the non-backing-side anode.

neutron momentum since the fragment energies are measured in coincidence post-neutron emission. While a 2E analysis to extract fission fragment masses could be performed on this data it would require considerable modifications to the waveform analysis of the grid signals which are not necessary for determining post-neutron $\overline{TKE}$.

After waveform processing of the anode signals, two main corrections were applied: one correcting for the average energy loss in the Pu target and the target backing material and another to correct for the small gain mismatch between the two sides of the detector. The backing side anode was explicitly gain matched to the non-backing-side anode. Figure 4 shows the backing and nonbacking anode distributions before [Fig. 4(a)] and after [Fig. 4(b)] both of these corrections. The cathode signal and grid signals had limits applied that excluded most nonfission events based on signal size. These corrected anode distributions were then summed to determine the uncalibrated $\overline{TKE}$. The calibration from raw pulse height to MeV was based on the most extensive dataset to date: that of Akimov *et al.* [3]. The minimum neutron energy of 0.5 MeV was chosen based on WNR neutron energy limits and the Akimov dataset range. The uncertainty of 100 keV in the Akimov result was included in our error analysis. Other contributions to the uncertainty of the average TKE result include statistical uncertainties and a neutron-energy-dependent uncertainty based on frame overlap of neutrons in the spectrum as measured by Tovesson and Hill [11].

Calculation of the neutron energy is based on an accurate measurement of the neutron time of flight. The neutron time of flight is measured relative to the T0 signal of the accelerator. Figure 5 shows the neutron time-of-flight spectrum at WNR flight path 90L. The timing resolution can be measured from the photofission peak observed at ~40 ns for the detector position on the flight path. A Gaussian fit to this peak gives a timing resolution of 1.6 ns FWHM. An absolute calibration of the flight path length was achieved with the use of a natural carbon filter placed upstream of the detector. The well-known strong resonance at 2.078 MeV from the neutron cross section on carbon was used to determine the flight path length between

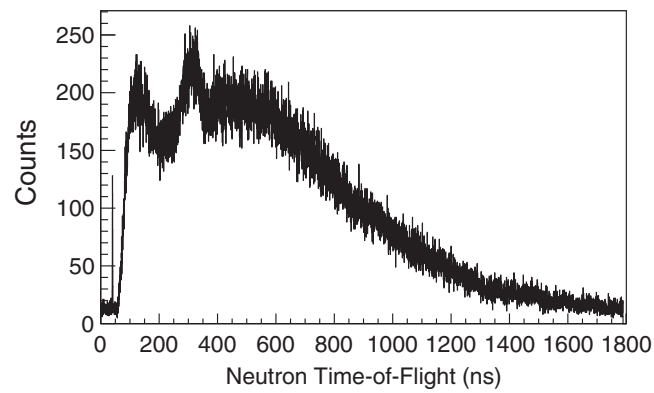

FIG. 5. Calibrated neutron time-of-flight distribution.

the spallation target and the ionization chamber. The flight path length for the experiment was calculated to be 12.00 ± 0.01 m.

The calibrated neutron time-of-flight spectrum is necessary for the neutron-energy-dependent analysis of the $\overline{TKE}$ of the plutonium fragments. Due to the pulsed nature of the beam at WNR, it is known that low-energy neutrons originating from one pulse can arrive in the subsequent pulse, leading to incorrect evaluation of their energy. Since the goal of this work is to determine the $\overline{TKE}$ as a function of neutron energy it is important to account for this misidentification of neutrons. The extent of this misidentification, or frame overlap, has been quantified by Ref. [11] for a ^{239}Pu target at WNR.

III. RESULTS AND DISCUSSION

The $\overline{TKE}$ measured for ^{239}Pu(n,f) as a function of incoming neutron energies between 0.5 and 50 MeV is shown in Fig. 6. This dataset significantly increases the range of energies as compared to previous measurements that were limited to a maximum value of 5.5 MeV in neutron energy [3]. The uncertainty in the $\overline{TKE}$ data has been calculated from statistical, calibration, and wraparound uncertainties. The uncertainty in the calibration results in 5–18% of the total uncertainty, the contribution from the wraparound correction is 0.1%, and the statistical uncertainty is the final and largest contributor. The horizontal error bars indicate the bin width in neutron energy. The uncertainty of each mean neutron energy is reported in Table I along with the $\overline{TKE}$ values. This work's extension of $\overline{TKE}$ to neutron energies above the second-, third-, and fourth- chance fission barriers is crucial to evaluating recent phenomenological fits by Madland and theoretical models by Lestone [4,5]. The dashed line in Fig. 6 is the linear fit produced by Madland based on previous data and limited to $E_n$ln 5.5 MeV. As can be seen in Fig. 6, while this fit still matches the region of data that it was originally intended for, the trend suggests it would not describe the data well in an extension to higher neutron energies. The dotted region of Fig. 6 is Lestone's model of $\overline{TKE}$ vs E_n up to 20 MeV. As argued in Lestone's work [5], the $\overline{TKE}$ of ^{239}Pu(n,f) is more accurately described by accounting for the energy dependence of multichance fission cross-sectional

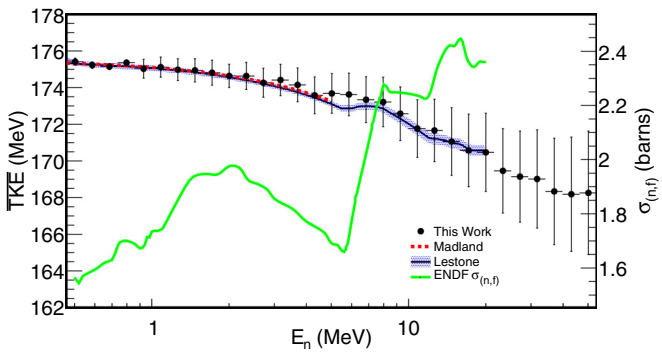

FIG. 6. Average total kinetic energy for fission products post-neutron emission for ^{239}Pu(n,f). Modeling predictions by Madland and Lestone and current ENDF/B-VII cross section of ^{239}Pu(n,f) are also plotted.

TABLE I. Measured $\overline{TKE}$ values for ^{239}Pu(n,f).

Mean E_n (MeV)	E_n bin width (MeV)	$\overline{TKE}$ (MeV)	Uncertainty $\overline{TKE}$ (MeV)
0.586 ± 0.023	0.090	175.2	0.2
0.683 ± 0.027	0.105	175.1	0.2
0.797 ± 0.032	0.122	175.4	0.2
0.929 ± 0.037	0.142	175.0	0.2
1.08 ± 0.04	0.16	175.1	0.2
1.26 ± 0.05	0.19	175.0	0.1
1.47 ± 0.06	0.23	174.9	0.1
1.71 ± 0.07	0.26	174.8	0.1
2.00 ± 0.08	0.31	174.6	0.1
2.33 ± 0.09	0.36	174.6	0.1
2.72 ± 0.11	0.42	174.3	0.1
3.17 ± 0.13	0.48	174.4	0.2
3.69 ± 0.15	0.57	174.1	0.2
4.31 ± 0.17	0.66	173.6	0.2
5.02 ± 0.20	0.77	173.7	0.2
5.86 ± 0.23	0.90	173.6	0.2
6.83 ± 0.27	1.05	173.3	0.2
7.97 ± 0.32	1.22	173.2	0.2
9.28 ± 0.37	1.42	172.6	0.2
10.8 ± 0.4	1.66	171.8	0.2
12.6 ± 0.5	1.93	171.7	0.2
14.7 ± 0.6	2.26	171.1	0.2
17.1 ± 0.7	2.63	170.6	0.2
20.0 ± 0.8	3.06	170.5	0.2
23.3 ± 0.9	3.57	169.5	0.2
27.2 ± 1.1	4.17	169.1	0.3
31.7 ± 1.3	4.86	168.0	0.3
36.9 ± 1.5	5.66	168.3	0.3
43.1 ± 1.7	6.60	168.2	0.3
50.2 ± 2.0	7.70	168.3	0.3

evaluations provided by ENDF/B-VII [12] (included in Fig. 6 for reference). These cross sections are predicted to turn on at different neutron energy thresholds, which are reflected in the $\overline{TKE}$ distribution as points of increasing $\overline{TKE}$ within the overall trend of decreasing $\overline{TKE}$ values with higher neutron energy. The data agree with the general trend of decreasing $\overline{TKE}$ with increasing neutron energy. Positions of second- and third-chance fission threshold predictions by Lestone are not readily discernible in the data set due to the size of the reported uncertainties in the $\overline{TKE}$ values as the largest source of uncertainty is the energy calibration; data collection from a known energy source such as ^{252}Cf could use known Cf $\overline{TKE}$ values to calibrate at higher neutron energies. Additionally, increased statistics which would allow for finer binning could also lead to investigation of the fission threshold regions.

IV. CONCLUSION

The extension of measured values of the $\overline{TKE}$ for ^{239}Pu(n,f) is shown for the first time here for neutron energies above 5.5 MeV. It is concluded that these measurements agree with the limited linear fit presented by Madland [4]

and broadly agree with the cross-section-based model by Lestone [5]. Further measurements of this system as well as independent energy calibration would aide in reducing measurement uncertainties and refinement of the data in the fission threshold regions. Additional important measurements of the fission fragments from ^{239}Pu(n, f) reaction should include studying $\overline{TKE}$ as a function of mass and charge, in addition to incident neutron energies.

[1] R. Yanez, L. Yao, J. King, and W. Loveland, Phys. Rev. C **89**, 051604 (2014).

[2] C. M. Zöller, Ph.D. thesis, Technische Hochschule Darmstadt, Damstadt, Germany, 1995 (unpublished).

[3] N. I. Akimov, V. G. Vorob'eva, V. N. Kabenin, N. P. Kolosov, B. D. Kuz'minov, A. I. Sergachev, L. D. Smirenkina, and M. Z. Tarasko, Yad. Fiz. **13**, 484 (1971) [Sov. J. Nucl. Phys. **13**, 272 (1971)].

[4] D. G. Madland, Nucl. Phys. A **772**, 113 (2006).

[5] J. P. Lestone and T. T. Strother, Nucl. Data Sheets **118**, 208 (2014).

[6] P. W. Lisowski and K. F. Schoenberg, Nucl. Instrum. Methods Phys. Res., Sect. A **562**, 910 (2006).

[7] *V1720 Technical Information Manual* [www.caen.it], revisised 25 July 2014.

[8] S. Mosby, F. Tovesson, A. Couture, D. L. Duke, V. Kleinrath, R. Meharchand, K. Meierbachtol, J. O'Donnell, B. Perdue, D. Richman, and D. Shields, Nucl. Instrum. Methods Phys. Res., Sect. A **757**, 75 (2014).

[9] Ch. Straede, C. Budtz-Jørgensen, and H.-H. Knitter, Nucl. Phys. A **462**, 85 (1987).

[10] F. Vivès, F.-J. Hambsch, H. Bax, and S. Oberstedt, Nucl. Phys. A **662**, 63 (2000).

[11] F. Tovesson and T. S. Hill, Nucl. Sci. Eng. **165**, 224 (2010).

[12] M. B. Chadwick, M. Herman, P. Obložinský, M. E. Dunn, Y. Danon, A. C. Kahler, D. L. Smith, B. Pritychenko, G. Arbanas, R. Arcilla, R. Brewer, D. A. Brown, R. Capot, A. D. Carlson, Y. S. Cho, H. Derrien, K. Guber, G. M. Hale, S. Hoblit, S. Holloway, T. D. Johnso, T. Kawano, B. C. Kiedrowski, H. Kim, S. Kunied, N. M. Larson, L. Leal, J. P. Lestone, R. C. Little, E. A. McCutchan, R. E. MacFarlane, M. MacInnes, C. M. Mattoon, R. D. McKnight, S. F. Mughabghab, G. P. A. Nobre, G. Palmiott, A. Palumbo, M. T. Pigni, V. G. Pronyaev, R. O. Sayer, A. A. Sonzogni, N. C. Summers, P. Talou, I. J. Thompson, A. Trkov, R. L. Vogt, S. C. van der Marck, A. Wallner, M. C. White, D. Wiarda, and P. G. Young, Nucl. Data Sheets **112**, 2887 (2011).